JCTC Journal of Chemical Theory and Computation

Article

Cite This: J. Chem. Theory Comput. 2019, 15, 4044−4055

pubs.acs.org/JCTC

All-Electron Quantum Monte Carlo with Jastrow Single Determinant Ansatz: Application to the Sodium Dimer

Kousuke Nakano,*[,†,‡] Ryo Maezono,[‡,¶] and Sandro Sorella*[,†]

[†]International School for Advanced Studies (SISSA), Via Bonomea 265, 34136, Trieste, Italy

[‡]School of Information Science, Japan Advanced Institute of Science and Technology (JAIST), Asahidai 1-1, Nomi, Ishikawa 923-1292, Japan

[¶]Computational Engineering Applications Unit, RIKEN, 2-1 Hirosawa, Wako, Saitama 351-0198, Japan

ABSTRACT: In this work, we report potential energy surfaces (PESs) of the sodium dimer calculated by variational (VMC) and lattice-regularized diffusion Monte Carlo (LRDMC). The VMC calculation is accurate for determining the equilibrium distance and the qualitative shape of the experimental PES. Remarkably, after the application of the LRDMC projection to this single determinant ansatz, namely, the Jastrow Antisymmetrized Geminal Power (JAGP), chemical accuracy (∼1 kcal/mol) is reached in the binding energy, and the obtained equilibrium internuclear distance and harmonic vibrational frequency are in very good agreement with the experimental ones. This outcome is crucially dependent on the quality of the optimization used to determine the best possible trial function within the chosen ansatz. The strategy adopted in this work is to minimize the variational energy by initializing the trial function with the density functional theory (DFT) single determinant ansatz expanded exactly in the same atomic basis used for the corresponding VMC and LRDMC calculations. This atomic basis is reshaped ad-hoc for QMC calculations. Indeed, we multiply the standard Gaussian-type atomic orbitals by a one-body Jastrow factor, satisfying, in this way, the electron−ion cusp conditions. In order to achieve these important advantages, we have defined a very efficient DFT algorithm in the mentioned basis, by estimating the corresponding matrix elements on a mesh, and by using a much finer mesh grid in the vicinity of nuclei.

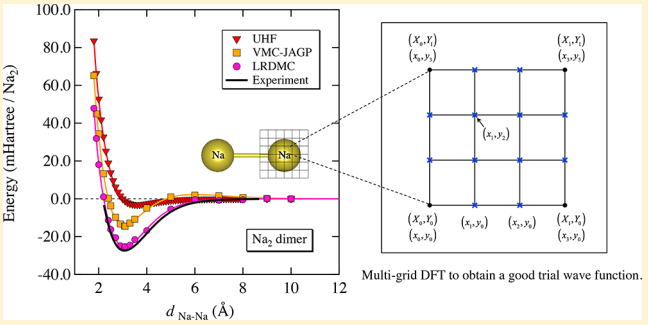

1. INTRODUCTION

First-principles quantum Monte Carlo (QMC) techniques, such as variational quantum Monte Carlo (VMC) and diffusion quantum Monte Carlo (DMC), are among the state-of-the-art numerical methods used to obtain highly accurate many-body wave functions.[1] Recent developments in QMC enable us to calculate not only the ground-state energy but also vibrational frequencies[2,3] and excited states,[4,5] as well as to study phase diagrams of materials[6] and determine quantitative properties of a metal−insulator transition[7] or excitonic behavior.[8] Because of the large computational cost, QMC can be easily applied only to model compounds such as atoms, small molecules, and simple crystals, and, so far, limited applications are known for complex electronic systems. However, it should be much more feasible and popular for "real materials" (e.g., protein, surface, glass, etc.) in the near future, because the QMC algorithm scales very well with the number N of electrons—at most, N^4—and sustains almost-ideal scaling in massively parallel architectures.[1]

In order to apply QMC for "real materials", it is convenient to replace core electrons with pseudopotentials because they have a little effect on chemical properties, and their replacement can reduce the QMC computational cost[9−11] by a factor proportional to $Z^{5.5-6.5}$, where Z is the atomic number. Nevertheless, all-electron calculations are important because they represent useful benchmarks for highly accurate methods, removing the problem to find very accurate pseudopotentials, though significant progress has been made recently.[12−17] Unfortunately, within QMC, all-electron calculations are rarely applied for atoms of large atomic number, mainly because they are too computationally demanding, at least in the simplest formulation of the VMC and DMC algorithms. Indeed, some progress has been obtained in VMC by considering more sophisticated trial moves in the Metropolis algorithm. Umrigar et al.[18,19] have proposed an accelerated Metropolis method to reduce fluctuations in the VMC methodology of full-core atoms, wherein electrons close to the atomic cores are displaced much more slowly than those in the valence region. Analogously, in DMC methodology,[1] the velocity is decreased only around nuclei, by improving the efficiency of the algorithm, compared with a standard all-electron calculation with a single very small time step. Moreover, a very accurate trial wave function is necessary for a reasonably efficient QMC all-electron simulation, because otherwise large absolute values of kinetic and potential energies around nuclei usually induce

Received: March 23, 2019
Published: May 22, 2019

large statistical fluctuations. For the latter problem, in this work, we determine the trial function by using a double-grid density functional theory (DFT) algorithm that is particularly accurate in the vicinity of the nuclei and can substantially reduce the energy fluctuations in the corresponding VMC and DMC calculations.

In order to obtain a good trial wave function, the Kohn−Sham Hamiltonian matrix elements involving a rapidly varying electron density (wave function) in the vicinity of nuclei should be accurately evaluated in DFT. The matrix elements are composed of integrals of the kinetic, the Coulomb (Hartree and electron−ion), and the exchange-correlation (XC) parts.[20] When the wave function is expanded using Gaussian-type orbitals (GTOs), integrals of the kinetic and the Coulomb parts can be determined analytically.[21] However, the integral should be determined numerically if the wave function is expanded in Slater-type orbitals (STOs), as well as in our modified GTO basis. In this case, Poisson's equation is solved to determine the Hartree potential by integrating the Coulomb kernel over the electron density calculated at each point of the mesh. This scheme is employed in our TurboRVB code.[22] If Poisson's equation is solved in real space (e.g., the finite element method[23]), the integral can be evaluated without any other approximation than the finite mesh. Moreover, an arbitrary fine mesh grid can be used in the vicinity of nuclei, within the so-called multigrid approach.[23] On the other hand, the multigrid approach is not easily implemented when the very efficient fast Fourier transform (FFT) is used to solve Poisson's equation. In this case, the grid should be *uniform* in all the space, which increases the computational cost. This drawback can be solved by the so-called pseudocharge method within the LAPW technique,[20,24] but the corresponding implementation is rather involved. In this work, we determine the Hartree potential with standard FFT convolution on a coarse mesh, then interpolate these values on a much finer mesh in the vicinity of nuclei. We show that this is enough to determine a good trial function that can be used as a suitable starting guess for QMC energy optimization. Although the DFT energy obtained with the above approximation is not exactly consistent with the one corresponding to a very dense uniform mesh, the QMC energies and the variances of the obtained initial trial wave functions are almost indistinguishable from each other. We emphasize that this is just due to the simple and efficient interpolation scheme of the Hartree potential that we have introduced in this work.

This method is applied to the sodium dimer, which has been extensively studied both experimentally[25−32] and theoretically[33−41] in the past decades. Several all-electron VMC and DMC studies have been reported for various atoms and molecules;[11,18,42−58] however, to our knowledge, only one paper has reported the sodium dimer,[56] wherein the dissociation energy at the experimental equilibrium distance has been calculated. Moreover, the full potential energy surface (PES) and other spectroscopic properties, such as harmonic vibration frequency, have not been calculated using all-electron VMC and DMC yet. All-electron calculations for the sodium dimer is informative as a reference, because it is known that the use of a pseudopotential sometimes induces discrepancies, because of the presence of the semicore electrons.[59] We successfully calculated PESs of the sodium dimer with small statistical errors, and the obtained dissociation energy, equilibrium internuclear distance, and harmonic vibrational frequency are in very good agreement with the experimental values. The main outcome of this work is that, after the optimization of the energy, a single determinant ansatz, the so-called JAGP described in the next section, can accurately describe this very weak and challenging chemical bond, within the QMC technique. This is very important because a single determinant ansatz can be extended to much larger systems, even within the computationally demanding QMC methods. In contrast, the multireference approach would be certainly impossible in this case, because it requires a number of determinants that is exponentially large in the number of electrons, and a corresponding computational burden.

2. METHODOLOGY

2.1. Variational and Lattice-Regularized Diffusion Monte Carlo. The Jastrow single determinant Ansatz, a Jastrow−Slater determinant (JSD), and Jastrow antisymmetrized geminal power (JAGP)[52] variational wave functions, are defined by the product of two terms, namely, a Jastrow factor and an antisymmetric part ($\Psi = J\Psi_{\mathrm{AGP/SD}}$). The Jastrow term is composed of one-body, two-body, and three/four-body factors ($J = J_1J_2J_{3/4}$). The one-body and two-body factors are used to fulfill the electron−ion and electron−electron cusp conditions, respectively. The one-body Jastrow factor is defined by:

$$J_1(\vec{r}_1, ..., \vec{r}_N) = \exp\left(\sum_{i,I,l} g_{I,l}\chi^J_{I,l}(\vec{r}_i)\right)\cdot\prod_i \tilde{J}_1(\vec{r}_i) \tag{1}$$

$$\tilde{J}_1(\vec{r}) = \exp\left[\sum_I -(2Z_I)^{3/4}u(2Z_I{}^{1/4}|\vec{r} - \vec{R}_I|)\right] \tag{2}$$

where $\vec{r}_i$ are the electron positions, R_I are the atomic positions with corresponding atomic number Z_I, l runs over atomic orbitals $\chi^J_{I,l}$ (e.g., GTO) centered on the atom I, and $u(r)$ contains a variational parameter b:

$$u(r) = \frac{b}{2}(1 - e^{-r/b}) \tag{3}$$

The two-body Jastrow factor reads as follows:

$$J_2(\vec{r}_1, ..., \vec{r}_N) = \exp\left(\sum_{i<j} v(r_{i,j})\right) \tag{4}$$

where $r_{i,j}$ is the distance between two electrons ($r_{i,j} = |\vec{r}_i - \vec{r}_j|$), and $v(r)$ contains a variational parameter F:

$$v(r) = \frac{r}{2}(1 - Fr)^{-1} \tag{5}$$

The three-body Jastrow factor is defined by:

$$J_{3/4}(\vec{r}_1, ..., \vec{r}_N) = \exp\left(\sum_{i<j} \Phi_J(\vec{r}_i, \vec{r}_j)\right) \tag{6}$$

$$\Phi_J(\vec{r}_i, \vec{r}_j) = \sum_{l,m,a,b} g^{a,b}_{l,m}\chi^J_{a,l}(\vec{r}_i)\chi^J_{b,m}(\vec{r}_j) \tag{7}$$

where the indices l and m again indicate different orbitals centered on corresponding atoms a and b. In the present study, the coefficients of the three/four-body Jastrow factor were set to zero in the case of $a \neq b$. The antisymmetric part has the following expression:

DOI: 10.1021/acs.jctc.9b00295
J. Chem. Theory Comput. 2019, 15, 4044−4055

Table 1. Basis Set Convergence for the Na Atom

basis set[a]	DFT-LDA[b] (Ha)	VMC-JDFT (Ha)	LRDMC (GF = JDFT) (Ha)	VMC-JSD[c] (Ha)	LRDMC (GF = JSD) (Ha)
cc-pVDZ + 1B Jastrow[d]	−161.42202	−162.20476(21)	−162.23790(35)	−162.21331(17)	−162.24031(22)
cc-pVTZ + 1B Jastrow[e]	−161.43238	−162.20879(32)	−162.24065(14)	−162.21350(16)	−162.24049(22)
cc-pVQZ + 1B Jastrow[f]	−161.43508	−162.20939(38)	−162.24065(15)	−162.21464(14)	−162.24102(21)

[a]1B Jastrow denotes $\tilde{J}_1$ in eq 26. [b]DFT-LDA calculations were performed using $(0.02\ \text{Bohr})^3$ fine grids. [c]The exponent parts were not optimized in these VMC-JSD calculations. [d]The basis set is composed of $9s8p1d$ ($Z \leq 306.4$), and the initial one-body parameter is $b = 1.1$. [e]The basis set is composed of $11s10p2d1f$ ($Z \leq 478.6$), and the initial one-body parameter is $b = 0.9$. [f]The basis set is composed of $13s12p3d2f1g$ ($Z \leq 542.5$), and the initial one-body parameter is $b = 0.7$.

Table 2. Ground-State Energies of the Na Atom Obtained by HF, VMC, and LRDMC, and the Estimated Exact Energy[a]

method	grid used in DFT-LDA	energy (Ha)	correlation (%)
HF	–	−161.8589[b]	0
VMC-JSD	–	−162.20717(33)[c]	88.01(8)
VMC-JAGP	–	−162.1434(7)[d]	71.9(2)
DMC (GF = JAGP)	–	−162.2370(1)[e]	95.6(3)
DMC (GF = STO-HF)	–	−162.23966(22)[f]	96.22(6)
DFT-LDA	Exact	−161.42178[g]	–
	$(0.02\ \text{Bohr})^3$	−161.42202	–
	$(0.05\ \text{Bohr})^3$	−165.57724	–
	$(0.10\ \text{Bohr})^3$	unstable	–
	$(0.05\ \text{Bohr})^3 + (0.01\ \text{Bohr})^3_{\text{cubic}}$	−161.55184	–
	$(0.10\ \text{Bohr})^3 + (0.01\ \text{Bohr})^3_{\text{cubic}}$	−162.97564	–
	$(0.20\ \text{Bohr})^3 + (0.01\ \text{Bohr})^3_{\text{cubic}}$	−173.13133	–
	$(0.20\ \text{Bohr})^3 + (0.01\ \text{Bohr})^3_{\text{linear}}$	−174.67558	–
VMC-JDFT	$(0.02\ \text{Bohr})^3$	−162.20476(21)	87.40(5)
	$(0.05\ \text{Bohr})^3$	−154.580(11)	–
	$(0.10\ \text{Bohr})^3$	unstable	–
	$(0.05\ \text{Bohr})^3 + (0.01\ \text{Bohr})^3_{\text{cubic}}$	−162.20437(19)	87.30(5)
	$(0.10\ \text{Bohr})^3 + (0.01\ \text{Bohr})^3_{\text{cubic}}$	−162.20258(20)	86.85(5)
	$(0.20\ \text{Bohr})^3 + (0.01\ \text{Bohr})^3_{\text{cubic}}$	−162.16962(28)	78.52(7)
	$(0.20\ \text{Bohr})^3 + (0.01\ \text{Bohr})^3_{\text{linear}}$	−162.16449(28)	77.23(7)
LRDMC (GF = JDFT)	$(0.02\ \text{Bohr})^3$	−162.23790(35)	95.78(9)
	$(0.05\ \text{Bohr})^3 + (0.01\ \text{Bohr})^3_{\text{cubic}}$	−162.23798(24)	95.80(6)
	$(0.10\ \text{Bohr})^3 + (0.01\ \text{Bohr})^3_{\text{cubic}}$	−162.23743(26)	95.66(6)
VMC-JSD	–	−162.21474(17)	89.93(4)
VMC-JAGP	–	−162.22079(16)	91.46(4)
LRDMC (GF = JSD)	–	−162.24078(20)	96.51(5)
LRDMC (GF = JAGP)	–	−162.24249(16)	96.94(4)
Exact	–	−162.2546[h]	100

[a]GF denotes the guiding function. [b]Data taken from ref 86. [c]Data taken from ref 55. [d]Data taken from ref 52. [e]Data taken from ref 52. [f]See the Supporting Information in ref 56. [g]Calculated by Gaussian 09 Revision E.01 with SPL/cc-pVDZ. [h]Data taken from ref 74.

$$\Psi_{\text{AGP}}(\vec{r}_1, ..., \vec{r}_N) = \det(\Phi_{\text{AGP}}(\vec{r}_i, \vec{r}_j)) \tag{8}$$

and the geminal function is expanded over atomic orbitals (e.g., GTO):

$$\Phi_{\text{AGP}}(\vec{r}_i, \vec{r}_j) = \sum_{l,m,a,b} \lambda_{a,b}^{l,m} \phi_{a,l}(\vec{r}_i)\phi_{b,m}(\vec{r}_j) \tag{9}$$

where indices l and m indicate different orbitals centered on atoms a and b, and i and j are coordinates of spin-up and spin-down electrons, respectively. The antisymmetric part can also be represented by molecular orbitals:[53]

$$\Phi_{\text{AGP}}(\vec{r}_i, \vec{r}_j) = \sum_{k}^{L} \lambda_k \tilde{\psi}_k(\vec{r}_i)\tilde{\psi}_k(\vec{r}_j) \tag{10}$$

$$\tilde{\psi}_k(\vec{r}) = \sum_{a}^{M} \sum_{l}^{L_a} c_{a,l}^{k} \phi_{a,l}(\vec{r}) \tag{11}$$

where M is the number of atoms, L_a is the number of atomic orbitals belonging to atom a, $c_{a,l}^{k}$ are the coefficients of the atomic orbitals, and L is the number of molecular orbitals. If L is equal to the half of the total number of electrons ($N/2$), the antisymmetric part coincides with the Slater determinant.[52,53] In this study, the cc-pVDZ basis set taken from the EMSL

DOI: 10.1021/acs.jctc.9b00295
J. Chem. Theory Comput. 2019, 15, 4044−4055

Basis Set Library[60,61] was used for the atomic orbitals for the determinant part (ϕ) of sodium both in JSD and JAGP ansatz. According to the scheme recently introduced by Mazzola et al.,[6] the orbitals whose exponents (Z) are larger than 306.4 were cut to avoid numerical instabilities. We note that the large exponent elements removed from the basis set are taken into account implicitly by means of the one-body Jastrow term[6] that indeed allows us to fulfill the electron−ion cusp conditions exactly. The atomic basis set used in this study is finally composed of $9s8p1d$ and $5s4p1d$ for the determinant part (ϕ) and the Jastrow factor (χ^J), respectively. These basis sets were treated as uncontracted ones. As shown in Table 1, although the cc-pVDZ basis is clearly poor for DFT-LDA, the corresponding VMC-JDFT[a] and LRDMC (GF = JDFT)[b] energies are just ∼3 mHa higher than the converged cc-pVQZ ones. The basis set errors of the cc-pVDZ become much smaller by optimizing the coefficients of the determinant part (i.e., JSD in Table 1), namely, ∼1.3 mHa and ∼0.7 mHa for VMC and LRDMC calculations, respectively. Remarkably, the JSD result also indicates that convergence to the complete basis set limit can be achieved more conveniently by optimizing the exponents of the small cc-pVDZ basis: Indeed, in this way, we obtain JSD energies of the cc-pVDZ basis (for VMC, −162.21474(17) Ha, and for LRDMC, −162.24078(20) Ha; see Table 2) that are statistically consistent with the ones corresponding to the much larger cc-pVQZ basis (for VMC, −162.21464(14) Ha, and for LRDMC, −162.24102(21) Ha; see Table 1). This result, on one hand, further supports the very fast convergence in the basis set for QMC methods; on the other hand, it clearly justifies the use of the *minimal* cc-pVDZ basis set (with optimization of exponents) in all the forthcoming QMC calculations with negligible basis set errors. The variational JSD and JAGP wave functions were optimized using the stochastic reconfiguration in combination with the linear method[62,63] that enable us to optimize thousands of parameters simultaneously even within a stochastic optimization technique. In this work, three types of VMC calculations were performed. VMC-JDFT denotes that only the Jastrow factor was optimized using the JSD ansatz, in which the g matrix elements in eqs 1 and 7, b in eq 3, and F in eq 5 are the variational parameters. On the other hand, all variational parameters in the Jastrow factor and the determinant part were optimized in VMC-JSD and VMC-JAGP calculations.

Lattice-regularized diffusion Monte Carlo (LRDMC) is a projection technique that allows a systematic improvement of the variational ansatz, yielding the corresponding one with the lowest energy and the same signs in configuration space. This energy is the so-called "fixed-node" DMC energy and can be obtained with the standard short time discretization,[18] i.e., the conventional approach, or by the so-called lattice regularization, namely, by discretizing on a lattice the continuous Hamiltonian.[64−66] We summarize the method here by emphasizing some important improvements for the all-electron case studied here. The interested readers should refer to refs 67−70 for details. In LRDMC, the original continuous Hamiltonian is regularized by an approximate one H^a, such that $H^a \to H$ for $a \to 0$, where a is the parameter used to discretize the continuous space. We consider the Hamiltonian in atomic units:

$$H = -\frac{1}{2}\sum_i^N \Delta_i + V(\vec{x}) + \sum_{I<J}\frac{Z_I Z_J}{|\vec{R}_I - \vec{R}_J|} \tag{12}$$

where N is the number of electrons, $\vec{x}$ is $3N$ dimension electron coordination, $\vec{x} = (\vec{r}_1, \vec{r}_2, ..., \vec{r}_N)$, and $V(\vec{x}) = V_{ee}(\vec{x}) + V_{ei}(\vec{x})$ is the standard many-body potential, which includes the electron−electron interaction:

$$V_{ee}(\vec{x}) = \sum_{i<j}\frac{1}{|\vec{r}_i - \vec{r}_j|} \tag{13}$$

and the electron−ion interaction:

$$V_{ei}(\vec{x}) = -\sum_i v_{ei}(\vec{r}_i) = -\sum_i\sum_I \frac{Z_I}{|\vec{r}_i - \vec{R}_I|} \tag{14}$$

where $\vec{R}$ and $\vec{r}$ are the ionic and electron positions, respectively. The kinetic part is approximated by a finite difference form:

$$\Delta_i \approx \Delta_i^a = \Delta_i^{a,p} + \Delta_i^{a',1-p} \tag{15}$$

where $\Delta_i^{a,p}$ is defined by a mesh size a and a function $p(\vec{r})$:

$$\Delta_i^{a,p} f(x_i, y_i, z_i) = \frac{1}{a^2}[p(x_i + a/2)(f(x_i + a) - f(x_i)) + p(x_i - a/2)(f(x_i - a) - f(x_i))] + x_i \leftrightarrow y_i \leftrightarrow z_i \tag{16}$$

In this work, we have adopted a more convenient and simpler form for the function $p(\vec{r})$ that is chosen as

$$p(\vec{r}) = \exp(-4|\vec{r} - \vec{R}_c|^2) \tag{17}$$

where $\vec{R}_c$ is the position of the nucleus closest to the electron at $\vec{r}$. The function p decays much faster than the original form ($p(\vec{r}) = 1/(1 + Z^2/4|\vec{r} - \vec{R}_c|^2)$) and enables us to use the larger lattice space a' in a wider valence region, because the small lattice space a is used only if the electron is very close to the nucleus. The constant a'/a is set to an irrational number in order to sample all the continuous space of the original Hamiltonian.[67] The potential term $V(x) = V_{ee}(x) + V_{ei}(x)$ is also discretized by the parameter a to realize a smooth convergence for $a \to 0$. The electron−electron potential is not necessarily discretized, but the electron−ion one is modified as

$$v_{ei}(\vec{r}_i) \to v^a_{\max,i}(\vec{x}) = \mathrm{Max}[v^a_{zv,i}(\vec{x}), v_{ei}(\vec{r}_i)] \tag{18}$$

$$v^a_{zv,i}(\vec{x}) = v_{ei}(\vec{r}_i) + \frac{(\nabla^2_{i,a} - \nabla_i^2)\Psi_G(\vec{x})}{2\Psi_G(\vec{x})} \tag{19}$$

where $\Psi_G(\vec{x})$ is a guiding function, and $\nabla^2_{i,a} = \Delta_i^a$. Although the electron−ion potential ($v_{ei}(\vec{r}_i)$) on the right-hand side of eq 18 was regularized by

$$v_{ei}(\vec{r}_i) = \sum_I \frac{Z_I}{\mathrm{Max}(|\vec{r}_i - \vec{R}_I|, a)} \tag{20}$$

to cut the Coulomb singularity at small distances, in this work, we have noticed that this regularization is not necessary within the so-called fixed-node approximation. This is because $v^a_{zv,i}(\vec{x})$ does not diverge even when the electron−ion distance is small. Therefore, eq 18 ensures the removal of the singularity unless in the vicinity of the nodal surface. The fixed-node approximation also removes this singularity and, therefore, the algorithm remains always stable, even without the use of eq 20. Now that the Hamiltonian is discretized, the efficient lattice

DOI: 10.1021/acs.jctc.9b00295
J. Chem. Theory Comput. 2019, 15, 4044−4055

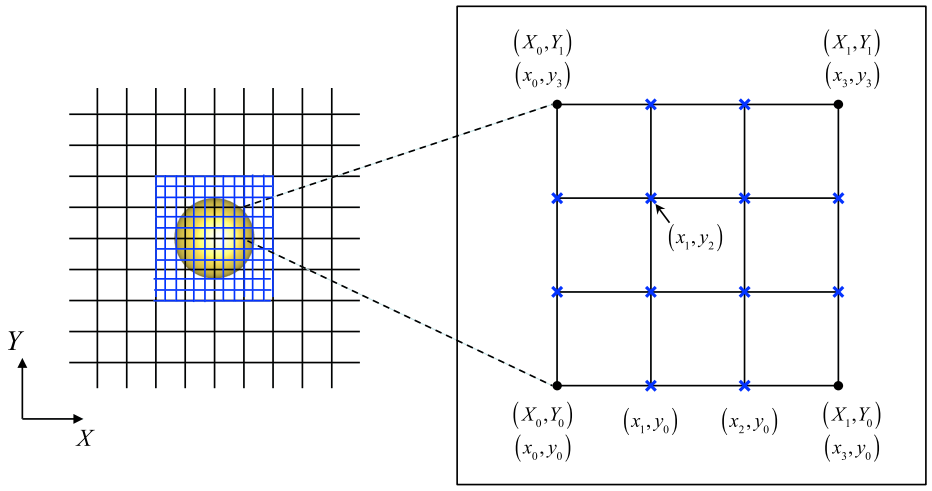

Figure 1. A two-dimensional schematic figure of the linear interpolation in the case of $n = 3$. The black dot (blue cross) marks in the right side figure represent the points on the coarse (interpolated) grid. The value of the Hartree potential on the interpolated grid $(x_1, y_2) \equiv (s_x = 1, s_y = 2)$ is estimated by the four nearest points in two-dimensional case as follows: $V_H(x_1,y_2) = \frac{2}{3}\cdot\frac{1}{3}V_H(X_0, Y_0) + \frac{1}{3}\cdot\frac{1}{3}V_H(X_1, Y_0) + \frac{2}{3}\cdot\frac{2}{3}V_H(X_0, Y_1) + \frac{1}{3}\cdot\frac{2}{3}V_H(X_1, Y_1)$.

Green function Monte Carlo algorithm,[64−66] which is valid on a lattice model, can be applied straightforwardly:

$$\langle x|H^a|\Psi_G\rangle = \sum_{x'} H^a_{x,x'}\langle x'|\Psi_G\rangle \tag{21}$$

The resulting algorithm is called LRDMC. The corresponding Green function matrix elements with the important sampling are $G_{x,x'} = \Psi_G(\vec{x}')(\Lambda_{x,x'} - H^a_{x',x})/\Psi_G(\vec{x})$, where Λ is a diagonal matrix with $\Lambda_{x,x} = \lambda$ and λ should be sufficiently large to obtain the ground state. The LRDMC algorithm is as follows:[67] given a walker with configuration $\vec{x}$ and weight w, a new configuration $x' \neq x$ is $p_{x,x'} = G_{x,x'}/b_x$, where $b_x = \sum_{x'\neq x} G_{x',x}$ is a normalization factor to make the Green function a transition probability. The walker weight is updated by a factor $w \rightarrow w\ \exp(-\tau_x e_L(\vec{x}, [\Psi_G]))$, where $\tau_x = -\log(rand)/b_x$ is a diffusion time determined by a random number $0 < rand \leq 1$, and $e_L(\vec{x}, [\Psi_G]) = \sum_{x'} H^a_{x',x}\Psi_G(\vec{x}')/\Psi_G(\vec{x})$ is the local energy corresponding to the guiding function Ψ_G. Of course, the usual branching scheme and many-walker technique can also be used. Unfortunately, the Green function cannot be made strictly positive for Fermions; therefore, the fixed-node approximation should be introduced.[70] To avoid the sign problem, the Hamiltonian is modified using the spin-flip term $\mathcal{V}_{SF}(\vec{x})$ (where $\mathcal{V}_{SF}(\vec{x}) = \sum_{x':s_{x,x'}>0} H_{x,x'}\Psi_G(\vec{x}')/\Psi_G(\vec{x})$):

$$H^{FN,\gamma}_{x,x'} = \begin{cases} H_{x,x} + (1+\gamma)\mathcal{V}_{SF}(\vec{x}) & \text{for } x' = x \\ H_{x,x'} & \text{for } x' \neq x,\ s_{x,x'} < 0 \\ -\gamma H_{x,x'} & \text{for } x' \neq x,\ s_{x,x'} > 0 \end{cases} \tag{22}$$

where $s_{x,x'} = \Psi_G(\vec{x})H_{x,x'}\Psi_G(\vec{x}')$ and $\gamma \geq 0$ is a real parameter. Finally, a mixed average of the fixed-node Hamiltonian,

$$E_{MA} = \frac{\langle\Psi_G|H^a_{FN}|\Upsilon_0\rangle}{\langle\Psi_G|\Upsilon_0\rangle} \tag{23}$$

can be calculated by the weights and local energies after sufficient number of projections, where $|\Upsilon_0\rangle$ is the ground-state wave function. The mixed average energy is consistent with the fixed-node energy of the standard DMC in the limit $a \rightarrow 0$.[67]

2.2. DFT Algorithm in the Same Basis Used for QMC.

The trial functions for the Jastrow single determinant ansatz were determined from DFT calculations by using a single determinant ansatz expanded exactly in the same atomic basis used for the corresponding VMC and LRDMC calculations. Within DFT, the Hamiltonian and the overlap matrix elements required for the solution of the Kohn−Sham equations are represented as

$$H^{a,b}_{i,j} = \int d\vec{r}\ \tilde{\phi}^b_j(\vec{r} - \vec{R}_b)\hat{H}(\vec{r})\tilde{\phi}^a_i(\vec{r} - \vec{R}_a) \tag{24}$$

$$S^{a,b}_{i,j} = \int d\vec{r}\ \tilde{\phi}^b_j(\vec{r} - \vec{R}_b)\tilde{\phi}^a_i(\vec{r} - \vec{R}_a) \tag{25}$$

where $\tilde{\phi}^a_i(\vec{r} - \vec{R}_a)$ and $\tilde{\phi}^b_j(\vec{r} - \vec{R}_b)$ are the ith, jth GTO for atoms a and b multiplied by a one-body Jastrow factor, namely,

$$\tilde{\phi}^b_j(\vec{r} - \vec{R}_b) = \phi^b_j(\vec{r} - \vec{R}_b)\tilde{J}_1(\vec{r}) \tag{26}$$

where $\tilde{J}_1(\vec{r})$ is the same as in eq 2. Indeed, as it is simple to show, each element of the basis set satisfies the so-called electron−ion cusp condition, namely, that when $\vec{r}$ is close to any atomic position $\vec{R}_b$:

$$\lim_{\vec{r}\rightarrow\vec{R}_b} \frac{\nabla\tilde{\phi}^a_j}{\tilde{\phi}^a_j} = -Z_b\frac{\vec{r} - \vec{R}_b}{|\vec{r} - \vec{R}_b|} \tag{27}$$

for all a, b. This formulation allows us to suppress the divergence of the local energy in the vicinity of nuclei in subsequent VMC and LRDMC calculations.

In order to construct the trial wave function efficiently, we have defined an efficient DFT algorithm in the mentioned basis, by estimating the corresponding matrix elements on a mesh, and by using a much finer mesh grid in the vicinity of nuclei. The Hamiltonian operator is composed of

$$\hat{H}(\vec{r}) = \hat{T} + V_H(\vec{r}) + V_{ext}(\vec{r}) + V_{XC}(\vec{r}) \tag{28}$$

where $\hat{T}$ is a kinetic operator, $V_H(\vec{r})$ is the Hartree (electron−electron) potential, $V_{ext}(\vec{r})$ is the electron−ion potential (that may or may not include a true external potential), and $V_{XC}(\vec{r})$ is the exchange-correlation potential. Given that the wave

DOI: 10.1021/acs.jctc.9b00295
J. Chem. Theory Comput. 2019, 15, 4044−4055

function is expanded in atomic orbitals such as GTO, the kinetic, electron−ion, and exchange-correlation terms are readily calculated at *any point in real space*. On the other hand, the Hartree potential is not determined in this manner, since it can be evaluated more conveniently on a uniform grid by solving Poisson's equation with FFT:

$$\nabla V_{\mathrm{H}}(\vec{r}) = -4\pi\rho(\vec{r}) \tag{29}$$

where $\rho(\vec{r})$ is the electron density. Therefore, the use of FFT with a fine grid in the vicinity of nuclei *necessarily* involves the same fine grid in the interstitial regions, where the electron density smoothly changes, which gratuitously increases the computational cost. In our implementation, we have found a good compromise between accuracy and efficiency in the following way. The Hartree potential is calculated first on a *coarse uniform grid* by solving Poisson's equation with the FFT algorithm. In the second step, the Hartree potential is interpolated on a *fine grid* only in the vicinity of nuclei, using standard interpolation methods, such as linear or cubic. A schematic figure of the linear interpolation in the two-dimensional case is shown in Figure 1. The values on the fine grid are interpolated using the nearest four points, namely,

$$\begin{aligned} V_{\mathrm{H}}(x_i, y_j) = {} & \left(1 - \frac{s_x}{n}\right)\cdot\left(1 - \frac{s_y}{n}\right)\cdot V_{\mathrm{H}}(X_I, Y_J) \\ & + \frac{s_x}{n}\cdot\left(1 - \frac{s_y}{n}\right)\cdot V_{\mathrm{H}}(X_{I+1}, Y_J) + \left(1 - \frac{s_x}{n}\right)\cdot\frac{s_y}{n}\cdot \\ & V_{\mathrm{H}}(X_I, Y_{J+1}) + \frac{s_x}{n}\cdot\frac{s_y}{n}\cdot V_{\mathrm{H}}(X_{I+1}, Y_{J+1}) \end{aligned} \tag{30}$$

where X_I and Y_J represent coarse grid points, $x_{i=nI+s_x}$ and $y_{j=nJ+s_y}$ represent interpolated points in the vicinity of nuclei, n is the ratio of the interpolated grid to the coarse one (i.e., $n - 1$ coincides with the number of interpolated fine points between the coarse-grid ones), and $0 \le s_x, s_y < n$. The values on the fine grid is interpolated by the nearest eight points in a three-dimensional case. The cubic interpolation is performed using the nearest 24 points. As a result, the matrix elements of the Hamiltonian can be evaluated by combining a coarse grid and an interpolated fine grid in the vicinity of nuclei. Notice that a similar interpolation was done in the pseudopotential calculation,[71,72] wherein the interpolation scheme was used to evaluate inner products between wave functions and nonlocal parts of pseudopotentials. The total DFT energy corresponding to the chosen interpolation for the Hartree potential is sizably different from the one obtained with a very fine grid (namely, converged). However, VMC and LRDMC energies obtained with the Kohn−Sham Slater determinants, with or without the interpolation scheme proposed, are very close, indicating that our DFT scheme provides very good Kohn−Sham orbitals, despite the observed error in the DFT energy.

3. VALIDATION OF THE INTERPOLATION SCHEME

To investigate the quality of the trial wave functions obtained by the interpolation technique, ground-state energies of the Na atom were calculated using DFT, VMC, and LRDMC. DFT calculations were performed with a single fine grid or using the interpolation scheme, wherein the LDA functional developed by Perdew and Zunger[73] was employed. Three types of single-grid DFT calculations were performed with $(0.02\ \mathrm{Bohr})^3$, $(0.05\ \mathrm{Bohr})^3$, and $(0.10\ \mathrm{Bohr})^3$ grids. For comparison, three types of DFT calculations using the cubic interpolation method were performed, namely, the $(0.01\ \mathrm{Bohr})^3$ grid was used for the core electron region, while the $(0.05\ \mathrm{Bohr})^3$, $(0.10\ \mathrm{Bohr})^3$, or $(0.20\ \mathrm{Bohr})^3$ grids were used for the valence electron region, wherein the core−electron region, centered on the Na atom, was chosen with a volume of $(2.00\ \mathrm{Bohr})^3$. The calculation using the linear interpolation method was also performed using $(0.01\ \mathrm{Bohr})^3$ and $(0.20\ \mathrm{Bohr})^3$ grids. Then, three types of VMC and LRDMC calculations were performed starting from the resultant wave functions. VMC-JDFT denotes that only the Jastrow factor was optimized using the Jastrow−Slater ansatz, namely, the nodal surface was determined by the DFT. VMC-JSD and VMC-JAGP denote that both the Jastrow factor and the determinant part were optimized using the Jastrow−Slater and Jastrow antisymmetrized geminal power ansatz, respectively. LRDMC (GF = JDFT, JSD, JAGP) denotes that the wave functions optimized using each ansatz were used for the guiding functions (GF). All results are summarized in Table 2.

In the fine grid calculations, without using the interpolation technique discussed above, a well-converged result was obtained only by using the $(0.02\ \mathrm{Bohr})^3$ single grid. Indeed, DFT calculation with the $(0.05\ \mathrm{Bohr})^3$ grid resulted in a much worse DFT-LDA and corresponding VMC-JDFT energies and a very coarse $(0.10\ \mathrm{Bohr})^3$ grid implies numerical instabilities. On the other hand, a very coarse $(0.10\ \mathrm{Bohr})^3$ grid is already sufficient to obtain a reasonable trial wave function when the cubic interpolation method is used. As expected, the DFT energy obtained by the interpolation method with $(0.10\ \mathrm{Bohr})^3$ + $(0.01\ \mathrm{Bohr})^3$ grids (−162.97564 Ha) is not consistent with that obtained by the very fine mesh (−161.42202 Ha), because of the approximation in the Hartree potential. However, the wave function obtained in this way can be used as a trial wave function for accurate VMC and DMC calculations, because the nodal surface is almost the same as the fine-grid one: The VMC-JDFT calculations (i.e., only the amplitude is optimized) show that the VMC energy obtained by the interpolation grid (−162.20258(20) Ha) is almost the same as the fine-grid one (−162.20476(21) Ha), where the deviation is only a few mHartree. The LRDMC (GF = JDFT) calculations also show a very good agreement [−162.23743(26) and −162.23790(35) Ha for the cubic interpolation and fine grid, respectively]. We stress that VMC-JDFT and LRDMC (GF = JDFT) energies obtained by the denser $(0.05\ \mathrm{Bohr})^3$ + $(0.01\ \mathrm{Bohr})^3$ grid are essentially consistent with those obtained using the $(0.02\ \mathrm{Bohr})^3$ single grid. Furthermore, our LRDMC (GF = JDFT) calculations also reproduce the reference energy (−162.23966(22) Ha) that was obtained by an all-electron DMC (GF = STO-HF) calculation using a very large basis set (quadruple-ξ-4-fold-polarized: QZ4P). These results indicate that the nodal surface determined by the interpolated DFT is as good as the fine-grid and the large-basis one. Thus, the interpolation method enables us to obtain a reasonable trial wave function with a low computational cost. Notice that, this interpolation method was applied also with $(0.20\ \mathrm{Bohr})^3$ and $(0.01\ \mathrm{Bohr})^3$ double mesh grids with much worse results as far as the quality of the nodal surface and corresponding VMC energies are concerned. Nevertheless, with such a sizable error, it can be clearly appreciated that the cubic interpolation performs better than the linear one.

The wave function can be further improved by optimizing the determinant part in the presence of the Jastrow factor. As

DOI: 10.1021/acs.jctc.9b00295
J. Chem. Theory Comput. 2019, 15, 4044−4055

shown in Table 2, VMC-JSD and VMC-AGP show lower variational energies than VMC-DFT, and LRDMC (GF = JSD, JAGP) also show lower variational energies than LRDMC (GF = JDFT) thanks to the improvement of the nodal surfaces. Remarkably, our LRDMC energy, corresponding to our best VMC-JAGP, is very close to the estimated exact total energy, namely, −162.2546 Ha.[74]

4. APPLICATION TO THE SODIUM DIMER

Potentail energy surfaces (PESs) of the sodium dimer were calculated by VMC-JAGP and LRDMC, by using the developed interpolation scheme, and were compared with previous experiments and calculations. First, a PES was calculated using JAGP ansatz by changing the internuclear distance from 1.8 Å to 10.0 Å; then, a PES was again calculated by LRDMC starting from the optimized wave functions. The energies obtained by LRDMC for each a were extrapolated by quartic polynomial fits $E(a) = E_0 + ba^2 + ca^4$ to obtain the $a \rightarrow 0$ limit (E_0), wherein a = 0.03, 0.04, 0.05, 0.06, 0.07, and 0.08 were employed (Figure 2) in all of these calculations. The

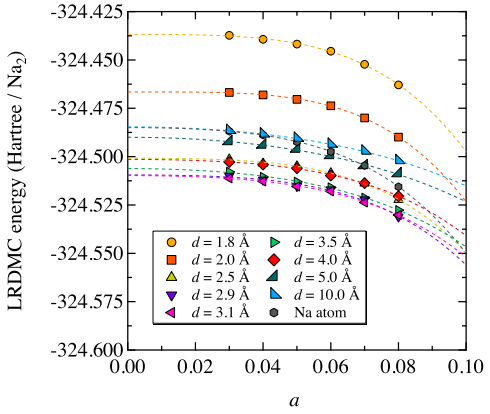

Figure 2. Total energy vs a in the LRDMC calculations of the sodium dimer. The energies labeled by Na atom are for two isolated Na atoms. The error bars are within the markers.

VMC-JAGP and LRDMC energies are summarized in Table 3, and the obtained PESs are shown in Figure 3. The PESs obtained using HF, MP2, CCSD(T)[c] calculated using Gaussian 09, Revision E.01,[75] and the experimental values reported by Verma et al.[30] are also shown in Figure 3 for comparison. Notice that the energy of the molecule at large distance coincides with twice the energy of a single atom, namely, the size consistency is perfectly fulfilled within VMC-JAGP and LRDMC calculations (see the bottom of Table 3).

We have analyzed the PESs, by using the simple analytic Murrell−Sorbie (MS) function[76] that has been widely used to describe the PES of neutral dimers,

$$E(\rho) = -D_e(1 + a_1\rho + a_2\rho^2 + a_3\rho^3)\exp(-a_1\rho) \quad (31)$$

where D_e is the dissociation energy without the zero-point vibration energy (ZPVE), $\rho = d - d_{eq}$, d is the internuclear distance between the sodium atoms, d_{eq} is the equilibrium internuclear distance, and a_1, a_2, and a_3 are fitting parameters. The D_e, d_{eq}, a_1, a_2, and a_3 were determined using the scipy.optimize.curve_fit module implemented in the Python SciPy library.[77] Then, harmonic vibration frequencies (ω_e (cm^{-1})) were calculated according to the following relationship:[38]

Table 3. Summary of the VMC-JAGP and LRDMC Calculations of the Sodium Dimer[a]

d_{Na-Na} (Å)	$E_{VMC-AGP}$ (Ha/Na_2)	E_{LRDMC} (Ha/Na_2)
1.8	−324.37708(34)	−324.43673(43)
1.9	−324.39731(25)	−324.45269(45)
2.0	−324.40784(33)	−324.46654(44)
2.2	−324.42894(27)	−324.48354(46)
2.4	−324.44191(22)	−324.49596(44)
2.5	−324.44593(30)	−324.50076(44)
2.7	−324.45197(25)	−324.50514(45)
2.9	−324.45554(25)	−324.50944(44)
3.0789	−324.45664(23)	−324.51033(44)
3.1	−324.45668(21)	−324.50982(43)
3.3	−324.45505(23)	−324.50911(44)
3.5	−324.45303(29)	−324.50616(44)
4.0	−324.44710(36)	−324.50139(44)
5.0	−324.44120(28)	−324.48999(43)
6.0	−324.44028(28)	−324.48502(42)
7.0	−324.44054(23)	−324.48538(42)
8.0	−324.44156(20)	−324.48511(43)
9.0	−324.44202(30)	−324.48443(42)
10.0	−324.44219(30)	−324.48459(43)
Na atom	−324.44158(32)	−324.48499(31)

[a]The energies labeled by Na atom are for two isolated Na atoms.

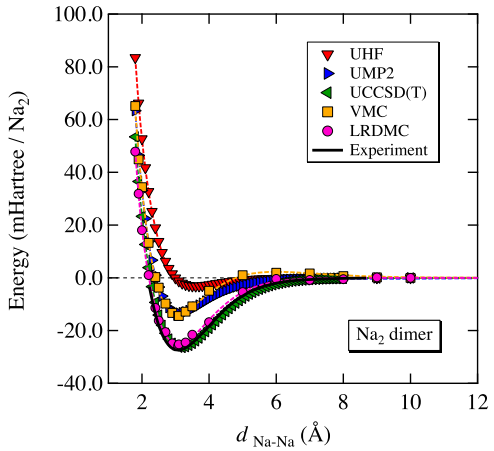

Figure 3. PESs of the sodium dimer. The broken lines show the obtained MS functions. The solid line shows the experimental values cited from ref 30. The error bars are within the markers.

$$\omega_e = \frac{1}{2\pi c}\sqrt{\frac{D_e(a_1^2 - 2a_2)}{\mu}} \quad (32)$$

where c is the light velocity and μ is the reduced mass. The obtained values are summarized in Table 4.

The VMC calculation reproduces the qualitative shape of the experimental PES (Figure 3), and is accurate for determining the equilibrium distance and the harmonic frequency (Table 4). However, it is not enough to obtain the accurate dissociation energy and reproduce the binding character in the range of 5.0−8.0 Å (i.e., showing higher energies than the dissociation limit). Notice that the VMC-JAGP is usually enough to reproduce almost correct binding energies for the second-row dimers.[78] This suggests that DMC is extremely important for molecules of large atomic number and that our Jastrow factor is not accurate enough to describe this weak chemical bond.

DOI: 10.1021/acs.jctc.9b00295
J. Chem. Theory Comput. 2019, 15, 4044−4055

Table 4. Summary of the Obtained Dissociation Energies, Equilibrium Distances, and Harmonic Vibrational Frequencies in This Work[a]

Method	D_e (mHa)	d_{eq} (Å)	ω_e (cm^{-1})
UHF	3.20	3.60	78.93
UCCSD(T)	26.49	3.179	154.82
QCISD[b]	26.53	3.181	151.63
VMC	13.57(10)	3.051(6)	155.5(1.7)
LRDMC	25.28(44)	3.083(11)	163.4(3.4)
Full valence CI[c]	26.85	3.09	159.1
Experiment[d]	27.44	3.08	159.1
Experiment[e]	26.82	3.079	159.12

[a]Values obtained by previous ab initio calculations and the experimental values are also listed. [b]Data taken from ref 38. D_e = 0.72193 (eV), d_{eq} = 0.31813 (nm), and ω_e = 151.63 (cm^{-1}); [c]Data taken from ref 33. D_e = 5892 (cm^{-1}), d_{eq} = 5.83 (Bohr), and ω_e = 159.1 (cm^{-1}); [d]Data taken from ref 79. D_e = 6022.6 (cm^{-1}), d_{eq} = 5.82 (Bohr), and ω_e = 159.1 (cm^{-1}); [e]Data taken from ref 80. D_e = 0.7298 (eV), d_{eq} = 0.3079 (nm), and ω_e = 159.12 (cm^{-1}).

The experimental PES is accurately described after the application of the LRDMC projection to the JAGP (Figure 3). The equilibrium distance (d_{eq} = 3.083(11) Å) and the harmonic frequency (ω_e = 163.4(3.4) cm^{-1}) obtained by our LRDMC calculations are very consistent with the experimental values (d_{eq} = 3.08 Å, ω_e = 159.1 cm^{-1}, and d_{eq} = 3.079 Å, ω_e = 159.12 cm^{-1}, taken from refs 79 and 80, respectively). The dissociation energy (D_e = 25.28(44) mHa) is also consistent with the experimental ones (D_e = 26.82 mHa (from ref 80) and D_e = 27.44 mHa (from ref 79)), and several theoretical works, such as coupled cluster calculations (D_e = 26.49 mHa for CCSD(T) and D_e = 26.53 mHa for QCISD (from ref 38)) and full valence configuration interaction calculation (D_e = 26.85 mHa (from ref 33)), converged within the chemical accuracy (~1 kcal/mol ≈ 1.6 mHa).

Although the deviation of the dissociation energy is small enough, it is worth discussing how to obtain a more-accurate result. In the work of Nemec et al.,[56] the deviation was argued to be due to insufficient nodal error cancellation between the atoms and the dimer. They reported that the dissociation energy of the sodium dimer was underestimated (D_e = 23.87(57) mHa at d = 3.0789 Å[d]) by an all-electron DMC calculation starting from STO.[56] The improvement in the error cancellation is important to obtain a more accurate result. In order to compare directly our results with the previous DMC one,[56] LRDMC (GF = JDFT, JSD, JAGP) calcuations for the sodium dimer at the same distance (d = 3.0789 Å) were performed. The results are shown in Figure 4 and are summarized in Table 5. LRDMC (GF = JDFT) and LRDMC (GF = JSD) give D_e = 23.64(63) mHa and D_e = 23.48(50) mHa, respectively, which are statistically consistent with the previous DMC calculation (D_e = 23.87(57) mHa). On the other hand, our LRDMC (GF = JAGP) greatly improves the error cancellation and provides, to our knowledge, the best binding energy (D_e = 25.34(54) mHa) so far available within QMC techniques. Figure 4 shows that the best variational energies are obtained when LRDMC is applied to the JAGP guiding functions both for the atom and the dimer, meaning that the corresponding nodal surfaces are better than previous calculations. Table 6 summarizes the absolute energies of the Na atom and dimer, as well as the residual errors in the absolute energies and corresponding binding energies within

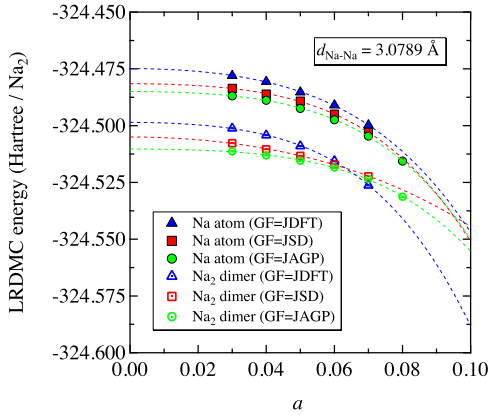

Figure 4. Total energy versus a in the LRDMC calculations of the sodium dimer at the experimental equilibrium distance (d_{Na-Na} = 3.0789 Å). The error bars are within the markers. GF denotes the guiding function.

Table 5. Dissociation Energies of the Sodium Dimer at the Experimental Equilibrium Distance (d_{Na-Na} = 3.0789 Å)

method	GF[a]	$E_{dimer-2atoms}$ (mHa)
DMC	STO-HF	23.87(57)[b]
LRDMC	JDFT	23.64(63)
LRDMC	JSD	23.48(50)
LRDMC	JAGP	25.34(54)

[a]GF denotes the guiding function. [b]14.981 ± 0.357 kcal/mol. See the Supporting Information of ref 56.

the fixed-node approximation. The nodal surface errors in LRDMC (GF = JSD) are 27.64 mHa and 30.98 mHa for two Na atoms and for the dimer, respectively. This implies 3.34 mHa smaller binding energy (D_e = 23.48(50) mHa) than the experimental value (D_e = 26.82 mHa) due to insufficient error cancellation. On the other hand, the nodal surface errors in LRDMC (GF = JAGP) become smaller, 24.21 mHa and 25.69 mHa for two Na atoms and the dimer, respectively, thanks to the multiconfigurational nature of JAGP[81,82] (i.e., static correlation). This leads to a much better binding energy (D_e = 25.34(54) mHa), because of the improvement in the error cancellation. Figure 5 shows the energy diagram and the results of the error cancellations. Compared to LRDMC (GF = JSD), LRDMC (GF = JAGP) reduces the nodal error for the two Na atoms by 3.43 mHa, while that for the dimer is reduced by 5.29 mHa, resulting in a better error cancellation and a corresponding more-accurate binding energy. While the value of ref 80 is used for the exact binding energy in this discussion, the conclusion does not change when the other experimental value (e.g., 27.44 mHa (from ref 79)) is employed. The fact that LRDMC (GF = JAGP) lowers the total energy more effectively in the dimer rather than in the atom indicates that the JSD nodes have some error also in the valence region, because one can assume an almost-exact nodal error cancellation in the core region.[56] Thus, we expect that the use of more-flexible wave functions such as backflow[83] or pfaffian[84] should further reduce the error and should lead to an almost-exact error cancellation (i.e., better binding energy) and essentially exact binding energies of dimers, as well as PESs.

DOI: 10.1021/acs.jctc.9b00295
J. Chem. Theory Comput. 2019, 15, 4044−4055

Table 6. Absolute Energies of the Sodium Atom and Dimer (d_{Na-Na} = 3.0789 Å) Obtained by LRDMC (GF = JSD, JAGP) and Experiments[a]

	LRDMC (GF = JSD)		LRDMC (GF = JAGP)		Experiment
	Energy (Ha)	NS error (mHa)	energy (Ha)	NS error (mHa)	exact energy (Ha)
2 Na atoms	−324.48156(40)	27.64	−324.48499(31)	24.21	−324.5092
dimer	−324.50504(30)	30.98	−324.51033(44)	25.69	−324.5360
D_e	23.48(50) (mHa)		25.34(54) mHa		26.82
NS error	3.34 mHa		1.48 mHa		–

[a]The nodal surface errors (NS errors) of the absolute energy and the binding energies due to the error cancellations are also shown. The exact energy of the Na atom and the exact binding energy are taken from refs 74 and 80, respectively. The exact energy of the sodium dimer was calculated from these values.

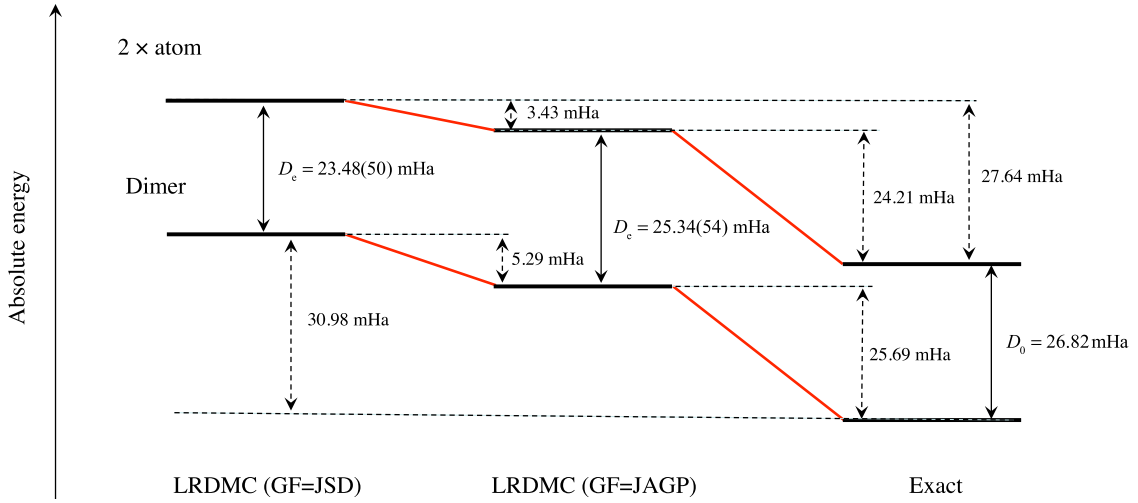

Figure 5. Diagram of the absolute energies of the Na atom and dimer. The nodal surface errors and the binding energies are also shown. The exact energy of the Na atom and the exact binding energy are taken from refs 74 and 80, respectively. The exact energy of the sodium dimer was calculated from these values.

5. SUMMARY

In this work, we report potential energy surfaces (PES) of the sodium dimer calculated by variational Monte Carlo (VMC) and lattice-regularized diffusion Monte Carlo (LRDMC) methods. Remarkably, after the application of the LRDMC projection to the Jastrow Antisymmetrized Geminal Power (JAGP) ansatz, chemical accuracy is reached in the binding energy, and the obtained equilibrium internuclear distance and harmonic vibration frequency are in good agreement with the experimental ones. The trial wave functions for the VMC and LRDMC calculations were prepared by the DFT single determinant ansatz expanded exactly in the same atomic basis used for the QMC calculation, which we have conveniently devised to satisfy the electron−ion cusp conditions exactly. We have found that the improvement in the description of the electron correlation and the weak chemical bond of the sodium dimer is mainly achieved thanks to the energy optimization strategy that we have developed in this work. For the all-electron calculation, the DFT step is computationally very demanding, at least in the convenient basis that we have chosen. Therefore, we have developed an efficient DFT algorithm in the mentioned basis, by estimating the corresponding matrix elements on a mesh, and by using a much finer mesh grid only in the vicinity of the nuclei. In this way, we can have a very good description of this chemical bond and evaluate the corresponding PES with a high degree of accuracy. We believe that our work represents an important step to define a quantum Monte Carlo method that will have the same reliability and accuracy of modern quantum chemistry packages in the future, with the considerable advantage that QMC with the single determinant ansatz used in this work scales very well with the number of electrons and has an almost-ideal scaling for massively parallel computations.

AUTHOR INFORMATION

Corresponding Authors

*E-mail: kousuke_1123@icloud.com (K. Nakano).
*E-mail: sorella@sissa.it (S. Sorella).

ORCID

Kousuke Nakano: 0000-0001-7756-4355

Notes

The authors declare no competing financial interest.

ACKNOWLEDGMENTS

The computations in this work have been mainly performed using the facilities of Research Center for Advanced Computing Infrastructure at Japan Advanced Institute of Science and Technology (JAIST). The structure of the sodium dimer was depicted by VESTA 3 package.[85] K.N. is grateful for financial support from the Simons Foundation. K.N. and S.S. are grateful for useful discussion with C. Genovese (SISSA). R.M. is grateful for financial support from MEXT-KAKENHI (Nos. 17H05478 and 16KK0097), FLAGSHIP2020 (Project Nos. hp180206 and hp180175 at K-computer), Toyota Motor Corporation, I−O DATA Foundation, and the Air Force

DOI: 10.1021/acs.jctc.9b00295
J. Chem. Theory Comput. 2019, 15, 4044−4055

Office of Scientific Research (No. AFOSR-AOARD/FA2386-17-1-4049).

■ ADDITIONAL NOTES

[a]VMC-JDFT denotes that only the Jastrow factor was optimized using the JSD ansatz.
[b]LRDMC and GF denote lattice-regularized diffusion Monte Carlo and the guiding function, respectively. See the next paragraph for details.
[c]The aug-cc-VQZ basis sets were used for these calculations.
[d]The original value is 14.918 ± 0.357 kcal/mol at d = 3.0789 Å. See the Supporting Information in ref 56.

■ REFERENCES

(1) Foulkes, W.; Mitas, L.; Needs, R.; Rajagopal, G. Quantum Monte Carlo simulations of solids. *Rev. Mod. Phys.* **2001**, *73*, 33.
(2) Luo, Y.; Zen, A.; Sorella, S. Ab initio molecular dynamics with noisy forces: Validating the quantum Monte Carlo approach with benchmark calculations of molecular vibrational properties. *J. Chem. Phys.* **2014**, *141*, 194112.
(3) Zen, A.; Luo, Y.; Sorella, S.; Guidoni, L. Molecular properties by Quantum Monte Carlo: an investigation on the role of the wave function ansatz and the basis set in the water molecule. *J. Chem. Theory Comput.* **2013**, *9*, 4332−4350.
(4) Mussard, B.; Coccia, E.; Assaraf, R.; Otten, M.; Umrigar, C. J.; Toulouse, J. *Advances in Quantum Chemistry*, Vol. *76*; Academic Press, 2018; pp 255−270.
(5) Hunt, R. J.; Szyniszewski, M.; Prayogo, G. I.; Maezono, R.; Drummond, N. D. Quantum Monte Carlo calculations of energy gaps from first principles. *Phys. Rev. B: Condens. Matter Mater. Phys.* **2018**, *98*, No. 075122.
(6) Mazzola, G.; Helled, R.; Sorella, S. Phase diagram of hydrogen and a hydrogen-helium mixture at planetary conditions by Quantum Monte Carlo simulations. *Phys. Rev. Lett.* **2018**, *120*, No. 025701.
(7) Stella, L.; Attaccalite, C.; Sorella, S.; Rubio, A. Strong electronic correlation in the hydrogen chain: A variational Monte Carlo study. *Phys. Rev. B: Condens. Matter Mater. Phys.* **2011**, *84*, 245117.
(8) Varsano, D.; Sorella, S.; Sangalli, D.; Barborini, M.; Corni, S.; Molinari, E.; Rontani, M. Carbon nanotubes as excitonic insulators. *Nat. Commun.* **2017**, *8*, 1461.
(9) Ceperley, D. The statistical error of green's function Monte Carlo. *J. Stat. Phys.* **1986**, *43*, 815−826.
(10) Hammond, B. L.; Reynolds, P. J.; Lester, W. A., Jr Valence quantum Monte Carlo with abinitio effective core potentials. *J. Chem. Phys.* **1987**, *87*, 1130−1136.
(11) Ma, A.; Drummond, N.; Towler, M.; Needs, R. All-electron quantum Monte Carlo calculations for the noble gas atoms He to Xe. *Phys. Rev. E* **2005**, *71*, No. 066704.
(12) Trail, J. R.; Needs, R. J. Correlated electron pseudopotentials for 3d-transition metals. *J. Chem. Phys.* **2015**, *142*, No. 064110.
(13) Krogel, J. T.; Santana, J. A.; Reboredo, F. A. Pseudopotentials for quantum Monte Carlo studies of transition metal oxides. *Phys. Rev. B: Condens. Matter Mater. Phys.* **2016**, *93*, 75143.
(14) Trail, J. R.; Needs, R. J. Shape and energy consistent pseudopotentials for correlated electron systems. *J. Chem. Phys.* **2017**, *146*, 204107.
(15) Bennett, M. C.; Melton, C. A.; Annaberdiyev, A.; Wang, G.; Shulenburger, L.; Mitas, L. A new generation of effective core potentials for correlated calculations. *J. Chem. Phys.* **2017**, *147*, 224106.
(16) Bennett, M. C.; Wang, G.; Annaberdiyev, A.; Melton, C. A.; Shulenburger, L.; Mitas, L. A new generation of effective core potentials from correlated calculations: 2nd row elements. *J. Chem. Phys.* **2018**, *149*, 104108.
(17) Annaberdiyev, A.; Wang, G.; Melton, C. A.; Chandler Bennett, M.; Shulenburger, L.; Mitas, L. A new generation of effective core potentials from correlated calculations: 3d transition metal series. *J. Chem. Phys.* **2018**, *149*, 134108.
(18) Umrigar, C. Accelerated metropolis method. *Phys. Rev. Lett.* **1993**, *71*, 408.
(19) Stedman, M.; Foulkes, W.; Nekovee, M. An accelerated Metropolis method. *J. Chem. Phys.* **1998**, *109*, 2630−2634.
(20) Martin, R. M. *Electronic Structure: Basic Theory and Practical Methods*; Cambridge University Press, 2004.
(21) Szabo, A.; Ostlund, N. *Modern Quantum Chemistry*; Macmillan Publishing Co., Inc., 1982.
(22) Sorella, S. TurboRVB:Quantum Monte Carlo Software for Electronic Structure Calculations. Available via the Internet at: https://people.sissa.it/~sorella/web, accessed March 10, 2019.
(23) Beck, T. L. Real-Space Mesh Techniques in Density Functional Theory. *Rev. Mod. Phys.* **2000**, *72*, 1041−1080.
(24) Singh, D. J. *Planewaves, Pseudopotentials and the LAPW Method*; Springer US: Boston, MA, 1994.
(25) Wood, R. W.; Hackett, F. E. The resonance and magnetic rotation spectra of sodium vapor photographed with the concave grating. *Astrophys. J.* **1909**, *30*, 339.
(26) Fredrickson, W. R. Rotational Structure of the Red Bands of Sodium. *Phys. Rev.* **1929**, *34*, 207.
(27) Demtröder, W.; McClintock, M.; Zare, R. N. Spectroscopy of Na_2 Using Laser-Induced Fluorescence. *J. Chem. Phys.* **1969**, *51*, 5495−5508.
(28) Demtröder, W.; Stock, M. Molecular constants and potential curves of Na_2 from laser-induced fluorescence. *J. Mol. Spectrosc.* **1975**, *55*, 476−486.
(29) Kusch, P.; Hessel, M. M. An analysis of the $B^1\Pi_u \rightarrow X^1\Sigma_g^+$ band system of Na_2. *J. Chem. Phys.* **1978**, *68*, 2591.
(30) Verma, K.; Bahns, J.; Rajaei-Rizi, A.; Stwalley, W. C.; Zemke, W. First observation of bound−continuum transitions in the laser-induced $A^1\Sigma_u^+ - X^1\Sigma_g^+$ fluorescence of Na_2. *J. Chem. Phys.* **1983**, *78*, 3599−3613.
(31) Kaminsky, M. E. New spectroscopic constants and RKR potential for the $A^1\Sigma_u^+$ state of Na_2. *J. Chem. Phys.* **1977**, *66*, 4951−4953.
(32) Qi, P.; Bai, J.; Ahmed, E.; Lyyra, A. M.; Kotochigova, S.; Ross, A. J.; Effantin, C.; Zalicki, P.; Vigú, J.; Chawla, G.; Field, R. W.; Whang, T. J.; Stwalley, W. C.; Knöckel, H.; Tiemann, E.; Shang, J.; Li, L.; Bergeman, T. New spectroscopic data, spin-orbit functions, and global analysis of data on the $A^1\Sigma_g^+$ and $b^3\Pi_u$ states of Na_2. *J. Chem. Phys.* **2007**, *127*, No. 044301.
(33) Magnier, S.; Millié, P.; Dulieu, O.; Masnou-Seeuws, F. Potential curves for the ground and excited states of the Na_2 molecule up to the (3*s*+5*p*) dissociation limit: Results of two different effective potential calculations. *J. Chem. Phys.* **1993**, *98*, 7113−7125.
(34) Ho, T. S.; Rabitz, H.; Scoles, G. Reproducing kernel technique for extracting accurate potentials from spectral data: Potential curves of the two lowest states $X^1\Sigma_g^+$ and $a^3\Sigma_u^+$ of the sodium dimer. *J. Chem. Phys.* **2000**, *112*, 6218−6227.
(35) Matsunaga, N.; Zavitsas, A. A. Comparison of spectroscopic potentials and an a priori analytical function. The potential energy curve of the ground state of the sodium dimer, $X^1\Sigma_g^+$ Na_2. *J. Chem. Phys.* **2004**, *120*, 5624−5630.
(36) Maroulis, G. Bonding and (hyper)polarizability in the sodium dimer. *J. Chem. Phys.* **2004**, *121*, 10519−10524.
(37) Harrison, J. F.; Lawson, D. B. Quadrupole moments of the alkali dimers, Li_2, Na_2, and K_2. *Int. J. Quantum Chem.* **2005**, *102*, 1087−1091.
(38) Ben-Hai, Y.; Qi-Run, D.; De-Heng, S.; Yu-Fang, L. Investigations on spectroscopic parameters, vibrational levels, classical turning points and inertial rotation and centrifugal distortion constants for the $X^1\Sigma_g^+$ state of sodium dimer. *Chin. Phys.* **2007**, *16*, 2962.
(39) Musiał, M.; Bartlett, R. J. Multi-reference Fock space coupled-cluster method in the intermediate Hamiltonian formulation for potential energy surfaces. *J. Chem. Phys.* **2011**, *135*, 044121.

DOI: 10.1021/acs.jctc.9b00295
J. Chem. Theory Comput. 2019, 15, 4044−4055

(40) Musial, M. Multireference Fock space coupled cluster method in the effective and intermediate Hamiltonian formulation for the (2,0) sector. *J. Chem. Phys.* **2012**, *136*, 134111.
(41) Morales, M. A.; McMinis, J.; Clark, B. K.; Kim, J.; Scuseria, G. E. Multideterminant wave functions in quantum Monte Carlo. *J. Chem. Theory Comput.* **2012**, *8*, 2181−2188.
(42) Reynolds, P. J.; Ceperley, D. M.; Alder, B. J.; Lester, W. A., Jr. Fixed-node quantum Monte Carlo for molecules. *J. Chem. Phys.* **1982**, *77*, 5593−5603.
(43) Reynolds, P.; Barnett, R.; Hammond, B.; Lester, W. Mol. Phys. and chemistry applications of quantum Monte Carlo. *J. Stat. Phys.* **1986**, *43*, 1017−1026.
(44) Vrbik, J.; DePasquale, M. F.; Rothstein, S. M. Estimating the relativistic energy by diffusion quantum Monte Carlo. *J. Chem. Phys.* **1988**, *88*, 3784−3787.
(45) Lester, W. A., Jr; Hammond, B. L. Quantum Monte Carlo for the electronic structure of atoms and molecules. *Annu. Rev. Phys. Chem.* **1990**, *41*, 283−311.
(46) Kenny, S.; Rajagopal, G.; Needs, R. Relativistic corrections to atomic energies from quantum Monte Carlo calculations. *Phys. Rev. A: At., Mol., Opt. Phys.* **1995**, *51*, 1898.
(47) Lüchow, A.; Anderson, J. B. First-row hydrides: Dissociation and ground state energies using quantum Monte Carlo. *J. Chem. Phys.* **1996**, *105*, 7573−7578.
(48) Yoshida, T.; Miyako, G. Diffusion quantum Monte Carlo calculation of positronium affinity of lithium. *J. Chem. Phys.* **1997**, *107*, 3864−3866.
(49) Huang, C.-J.; Umrigar, C.; Nightingale, M. Accuracy of electronic wave functions in quantum Monte Carlo: The effect of high-order correlations. *J. Chem. Phys.* **1997**, *107*, 3007−3013.
(50) Shlyakhter, Y.; Sokolova, S.; Lüchow, A.; Anderson, J. B. Energetics of carbon clusters C_8 and C_{10} from all-electron quantum Monte Carlo calculations. *J. Chem. Phys.* **1999**, *110*, 10725−10729.
(51) Sarsa, A.; Boronat, J.; Casulleras, J. Quadratic diffusion Monte Carlo and pure estimators for atoms. *J. Chem. Phys.* **2002**, *116*, 5956−5962.
(52) Casula, M.; Sorella, S. Geminal wave functions with Jastrow correlation: A first application to atoms. *J. Chem. Phys.* **2003**, *119*, 6500−6511.
(53) Casula, M.; Attaccalite, C.; Sorella, S. Correlated geminal wave function for molecules: An efficient resonating valence bond approach. *J. Chem. Phys.* **2004**, *121*, 7110−7126.
(54) Caffarel, M.; Daudey, J.-P.; Heully, J.-L.; Ramírez-Solís, A. Towards accurate all-electron quantum Monte Carlo calculations of transition-metal systems: Spectroscopy of the copper atom. *J. Chem. Phys.* **2005**, *123*, No. 094102.
(55) Buendía, E.; Gálvez, F.; Sarsa, A. Correlated wave functions for the ground state of the atoms Li through Kr. *Chem. Phys. Lett.* **2006**, *428*, 241−244.
(56) Nemec, N.; Towler, M. D.; Needs, R. Benchmark all-electron ab initio quantum Monte Carlo calculations for small molecules. *J. Chem. Phys.* **2010**, *132*, No. 034111.
(57) Scemama, A.; Applencourt, T.; Giner, E.; Caffarel, M. Accurate nonrelativistic ground-state energies of 3*d* transition metal atoms. *J. Chem. Phys.* **2014**, *141*, 244110.
(58) Powell, A. D.; Dawes, R. Calculating potential energy curves with fixed-node diffusion Monte Carlo: CO and N_2. *J. Chem. Phys.* **2016**, *145*, 224308.
(59) Maezono, R.; Towler, M.; Lee, Y.; Needs, R. Quantum Monte Carlo study of sodium. *Phys. Rev. B: Condens. Matter Mater. Phys.* **2003**, *68*, 165103.
(60) Feller, D. The role of databases in support of computational chemistry calculations. *J. Comput. Chem.* **1996**, *17*, 1571−1586.
(61) Schuchardt, K. L.; Didier, B. T.; Elsethagen, T.; Sun, L.; Gurumoorthi, V.; Chase, J.; Li, J.; Windus, T. L. Basis Set Exchange: A Community Database for Computational Sciences. *J. Chem. Inf. Model.* **2007**, *47*, 1045−1052.
(62) Sorella, S.; Casula, M.; Rocca, D. Weak binding between two aromatic rings: Feeling the van der Waals attraction by quantum Monte Carlo methods. *J. Chem. Phys.* **2007**, *127*, No. 014105.
(63) Umrigar, C. J.; Toulouse, J.; Filippi, C.; Sorella, S.; Hennig, R. G. Alleviation of the Fermion-sign problem by optimization of many-body wave functions. *Phys. Rev. Lett.* **2007**, *98*, 110201.
(64) Ten Haaf, D. F.; Van Bemmel, H. J.; Van Leeuwen, J. M.; Van Saarloos, W.; Ceperley, D. M. Proof for an upper bound in fixed-node Monte Carlo for lattice fermions. *Phys. Rev. B: Condens. Matter Mater. Phys.* **1995**, *51*, 13039−13045.
(65) Calandra Buonaura, M.; Sorella, S. Numerical study of the two-dimensional Heisenberg model using a Green function Monte Carlo technique with a fixed number of walkers. *Phys. Rev. B: Condens. Matter Mater. Phys.* **1998**, *57*, 11446−11456.
(66) Sorella, S.; Capriotti, L. Green function Monte Carlo with stochastic reconfiguration: An effective remedy for the sign problem. *Phys. Rev. B: Condens. Matter Mater. Phys.* **2000**, *61*, 2599−2612.
(67) Casula, M.; Filippi, C.; Sorella, S. Diffusion Monte Carlo method with lattice regularization. *Phys. Rev. Lett.* **2005**, *95*, 1−5.
(68) Casula, M.; Sorella, S.; Senatore, G. Ground state properties of the one-dimensional Coulomb gas using the lattice regularized diffusion Monte Carlo method. *Phys. Rev. B: Condens. Matter Mater. Phys.* **2006**, *74*, 245427.
(69) Casula, M.; Moroni, S.; Sorella, S.; Filippi, C. Size-consistent variational approaches to non-local pseudopotentials: Standard and lattice regularized diffusion Monte Carlo methods revisited. *J. Chem. Phys.* **2010**, *132*, 154113.
(70) Becca, F.; Sorella, S. *Quantum Monte Carlo Approaches for Correlated Systems*; Cambridge University Press, 2017.
(71) Ono, T.; Hirose, K. Timesaving double-grid method for real-space electronic-structure calculations. *Phys. Rev. Lett.* **1999**, *82*, 5016−5019.
(72) Ono, T.; Hirose, K. Real-space electronic-structure calculations with a time-saving double-grid technique. *Phys. Rev. B: Condens. Matter Mater. Phys.* **2005**, *72*, 085115.
(73) Perdew, J. P.; Zunger, A. Self-interaction correction to density-functional approximations for many-electron systems. *Phys. Rev. B: Condens. Matter Mater. Phys.* **1981**, *23*, 5048−5079.
(74) Chakravorty, S. J.; Gwaltney, S. R.; Davidson, E. R.; Parpia, F. A.; p Fischer, C. F. Ground-state correlation energies for atomic ions with 3 to 18 electrons. *Phys. Rev. A: At., Mol., Opt. Phys.* **1993**, *47*, 3649−3670.
(75) Frisch, M.; Trucks, G.; Schlegel, H.; Scuseria, G.; Robb, M.; Cheeseman, J.; Scalmani, G.; Barone, V.; Mennucci, B.; Petersson, G. A., et al. *Gaussian 09, Revision E.01*; Gaussian, Inc.: Wallingford, CT, 2013.
(76) Sorbie, K.; Murrell, J. Analytical potentials for triatomic molecules from spectroscopic data. *Mol. Phys.* **1975**, *29*, 1387−1407.
(77) Jones, E.; Oliphant, T.; Peterson, P., et al. SciPy: Open source scientific tools for Python. Available via the Internet at: http://www.scipy.org, accessed March 10, 2019.
(78) Marchi, M.; Azadi, S.; Casula, M.; Sorella, S. Resonating valence bond wave function with molecular orbitals: Application to first-row molecules. *J. Chem. Phys.* **2009**, *131*, 154116.
(79) Liu, Z.; Carter, L. E.; Carter, E. A. Full configuration interaction molecular dynamics of Na_2 and Na_3. *J. Phys. Chem.* **1995**, *99*, 4355−4359.
(80) Huber, K.-P. *Molecular Spectra and Molecular Structure: IV. Constants of Diatomic Molecules*; Springer Science & Business Media, 2013.
(81) Zen, A.; Coccia, E.; Luo, Y.; Sorella, S.; Guidoni, L. Static and dynamical correlation in diradical molecules by quantum monte carlo using the jastrow antisymmetrized geminal power ansatz. *J. Chem. Theory Comput.* **2014**, *10*, 1048−1061.
(82) Genovese, C.; Meninno, A.; Sorella, S. Assessing the accuracy of the Jastrow antisymmetrized geminal power in the H_4 model system. *J. Chem. Phys.* **2019**, *150*, No. 084102.

DOI: 10.1021/acs.jctc.9b00295
J. Chem. Theory Comput. 2019, 15, 4044−4055

(83) López Ríos, P.; Ma, A.; Drummond, N. D.; Towler, M. D.; Needs, R. J. Inhomogeneous backflow transformations in quantum Monte Carlo calculations. *Phys. Rev. E* **2006**, *74*, 066701.
(84) Bajdich, M.; Mitas, L.; Drobný, G.; Wagner, L. K.; Schmidt, K. E. Pfaffian pairing wave functions in electronic-structure quantum Monte Carlo simulations. *Phys. Rev. Lett.* **2006**, *96*, 130201.
(85) Momma, K.; Izumi, F. VESTA 3 for three-dimensional visualization of crystal, volumetric and morphology data. *J. Appl. Crystallogr.* **2011**, *44*, 1272−1276.
(86) Schäfer, A.; Horn, H.; Ahlrichs, R. Fully optimized contracted Gaussian basis sets for atoms Li to Kr. *J. Chem. Phys.* **1992**, *97*, 2571−2577.

DOI: 10.1021/acs.jctc.9b00295
J. Chem. Theory Comput. 2019, 15, 4044−4055